XMM OBSERVATIONS OF THE WR+O SYSTEM GAMMA VELORUM

T. Dumm[1], M. Güdel[2], W. Schmutz[3], M. Audard[2], H. Schild[1], M. Leutenegger[4], and K. van der Hucht[5]

[1]Institute for Astronomy, ETH Zentrum, CH-8092 Zürich, Switzerland
[2]Paul Scherrer Institut, CH-5232 Villigen PSI, Switzerland
[3]Physikalisch-Meteorologisches Observatorium Davos, CH-7260 Davos Dorf, Switzerland
[4]Department of Physics and Columbia Astrophysics Laboratory, Columbia University, New York, NY 10027, USA
[5]Space Research Organization Netherlands, NL-3584 Utrecht, The Netherlands

Abstract

We present *XMM-Newton* observations of the system γ Velorum at the two phases 0.1 and 0.4. The variation of the hard X-rays are interpreted as due to occultation by the WR wind. From a comparison of the observed intensity ratio to one predicted by an unclumped wind model we derive a clumping factor of 16 for the WR wind. We unequivocally identify two X-ray emitting regions: The shock zone of colliding stellar winds with temperatures up to 25 MK and a photoionized region with $T_e < 60$ kK. The revealing detection of the photoionized region is a narrow radiative recombination continuum of C VI at 25.3 Å. We suspect that shocks intrinsic to the stellar wind are a third type of X-ray source in the system and we tentatively identify the Ne IX line at 13.5 Å with this region.

Key words: Missions: XMM-Newton – stars: early-type – stars: winds, outflows – stars: Wolf-Rayet – x-rays: individual: γ Vel

1. Introduction

The system γ Velorum is a spectroscopic binary with a O 7.5 primary and a WC 8 secondary. Due to the proximity of γ Vel the object is a bright X-ray source and has been observed by all previous X-ray satellites from the *Einstein* observatory to *ASCA* and most recently, by *Chandra* (Skinner et al. 2001). With 13 *ROSAT* observations covering the binary orbit of γ Vel, Willis et al. (1995) detected that the hard X-ray emissivity is enhanced about a factor of 10 for a brief time period only, shortly after conjunction when the O star is in front. Willis et al. (1995) convincingly interpreted the variable hard X-ray emission to arise from colliding stellar winds. The enhancement is explained by the viewing geometry when the collision zone can be seen through a rarified cavity that builds around the O star and which points away from the Wolf-Rayet star. At other phases the WR wind completely absorbs the X-rays from the collision zone. The soft X-ray flux remains constant at all binary phases.

The orbital parameters of γ Vel are given by Schmutz et al. (1997), the stellar parameters of the O component by De Marco & Schmutz (1999), and those of the WR component by De Marco et al. (2000). *Hipparcos* observations yield a distance of 258^{+41}_{-31} pc (Schaerer et al. 1997; van der Hucht et al. 1997).

In this paper we report four observations with the *XMM-Newton* observatory of γ Vel, at phases 0.1 and 0.4. Spectra are obtained with the Reflection Grating Spectrometer (RGS) which are the first high resolution X-ray spectra of this object in the range 14 to 37 Å. In the next section we present the observations and then we analyze the high and low energy component in Sections 3 and 4, respectively. In Section 4 we discuss the implications of our observations.

2. Observations

XMM-Newton observed γ^2 Velorum at four occasions (see Tab. 1) using all its X-ray instruments, the European Photon Imaging Cameras (EPIC) MOS and PN simultaneous with both high-resolution Reflection Grating Spectrometers (RGS). For information on *XMM-Newton* and its X-ray instruments, we refer to the publications by den Herder et al. (2001), Jansen et al. (2001), Stüder et al. (2001), and Turner et al. (2001). Two observations where obtained each at the phases $\phi = 0.1$ and $\phi = 0.4$. Within the error bars we did not detect any differences between the spectra obtained at the same orbital positions. The observations at phase 0.1 has been obtained a few days after conjunction and the observations were scheduled such to observe the maximum according to the variations of X-ray intensities with orbital phase (Willis et al. 1995). The second phase is around quadrature when the X-ray flux is low. The geometry of the observations is illustrated in Fig. 1.

The data have been reduced with standard procedures using the *XMM-Newton* Science Analysis System (SAS) in conjunction with the latest calibration available (June 2001). The EPIC response matrices from the EPIC instrument team have been used to fit the CCD spectra. The RGS1 and RGS2 spectra have been co-added and "fluxed" using a wavelength grid with a step size of 51 mÅ.

In Fig. 2 we display the low resolution EPIC spectra at low and high state. The high state spectrum shows the signature of attenuation below 2 keV and the quadrature observations are absorbed for energies below 4 keV. At energies below 1 keV there is X-ray emission that is (almost) not variable between the two phases and between 1 and 2

Proc. Symposium *'New Visions of the X-ray Universe in the XMM-Newton and Chandra Era'* 26–30 November 2001, ESTEC, The Netherlands
ESA SP-488, August 2002 eds. F. Jansen & TBD

Table 1. Log of γ^2 Velorum observations by XMM-Newton. The R-number gives the satellite revolution number and the exposure time is given in hours. The phase ϕ is calculated according to the ephemeris of Schmutz et al. (1997), where the O star is in front at $\phi = 0.03$.

	high state $\phi = 0.12$ R #168 8-11-2000	low state $\phi = 0.34$ R #177 26-11-2000	high state $\phi = 0.11$ R #247 14-4-2001	low state $\phi = 0.37$ R #257 5-5-2001
Start [UT]	19:50	06:45	10:35	9:20
Instr.	Exp.T.	Exp.T.	Exp.T.	Exp.T.
RGS1	4.29	5.80	8.72	16.81
RGS2	4.51	5.80	8.72	16.81
MOS1	3.76	5.74	8.56	16.64
MOS2	3.83	5.77	8.56	16.64
PN	2.78	4.16	7.83	15.14

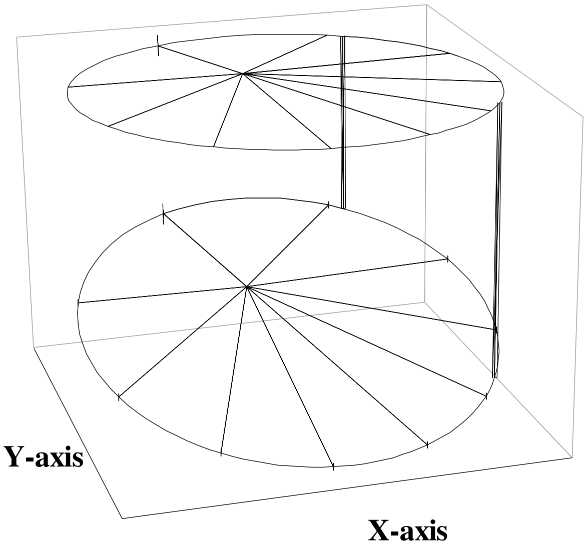

Figure 1. Orbit of the O star (lower ellipse) relative to the WR star which is fixed at the focus. Every 0.1 phase-interval there is a line connecting the two stellar positions. Periastron ($\phi = 0$) is indicated by a short vertical line. The projection of the orbit on the sky is shown by the upper ellipse at the top of the 3D-box. The two line of sights from $z = +\infty$ towards the O star is indicated by the two thick lines connecting the orbital ellipse with the projected one at the top. The observations have been obtained at the phases $\phi = 0.11$ and 0.37, respectively.

keV (12 and 6 Å) this presumably constant component is declining. In the high resolution RGS spectra, displayed in Fig. 3, it can be seen that what appears as a continuum below 2 keV (above 6 Å) in the low resolution EPIC spectra is in reality a pure emission line spectrum. Most lines below 1 keV remain unaffected by the orbital phase whereas above 1 keV the contribution from unabsorbed emission lines are a small fraction of the total emission. E.g. the Ne X λ12 line is reduced by a factor of about 4 and the Mg XI λ9.2 line by a factor of 10. At energies above

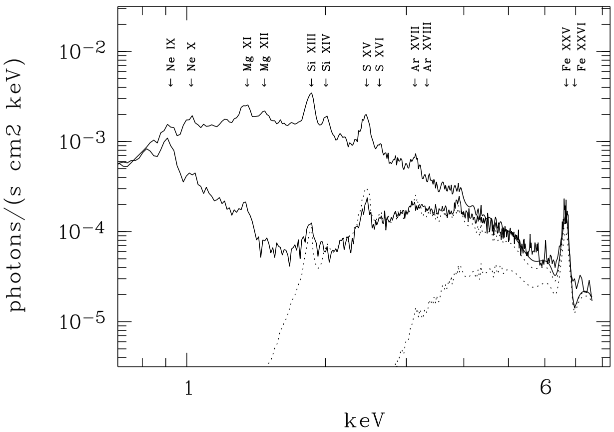

Figure 2. EPIC MOS data at low and high state. Also shown by the dotted line is the high state spectrum absorbed by the predicted column density due to the material of the WR wind along the line of sight towards the O star at phase $\phi = 0.37$ (see text). The second dotted line that fits closely the low state spectrum above 2 keV has been obtained by reducing the predicted column density by a factor of 4.

1 keV there is also continuum radiation in the high state spectrum as proven by the high resolution observations with *Chandra* (Skinner et al. 2001).

3. Variability of the high energy emission

If we fit the high state PN and MOS spectra above 0.95 keV (the Ne IX line is excluded) with a model of emission from a hot, optically thin plasma (enhanced MEKAL in SPEX90) then we find maximum plasma temperatures slightly above 2 keV. This maximum temperature is firm because Fe XXVI is at least a factor of 10 weaker than the observed Fe XXV (see Fig. 2). Therefore, we can exclude temperatures of the order of 10^8 K (8 keV) as predicted for the center of the wind-wind collision zone by hydrodynamic calculations (Walder et al. 1999). This discrepancy is expected because the quoted simulations neglect the effects of thermal transport (Folini & Walder 2000).

From previous observations we know that the high state of X-ray emission lasts for a brief interval only around phase $\phi = 0.1$. We follow the interpretation of Willis et al. (1995) and Stevens et al. (1996) in that we assume the high energy X-rays to emerge from the wind-wind collision zone and these X-rays are attenuated by the surrounding material of the WR wind, except for the phase when we view the collision zone through the cavity around the O star. Thus, in this interpretation the attenuation of the X-rays, i.e. the ratio of low to high state, is a linear measure of the column density of the WR wind.

In Fig. 2 we indicate with the doted line the predicted attenuation at phase 0.37. The energy spectrum of the low state is predicted by adopting the density structure of the WR wind as modeled by De Marco et al. (2000). We cacluate the column density towards the location of the O star as seen by an observer at phase $\phi = 0.37$,

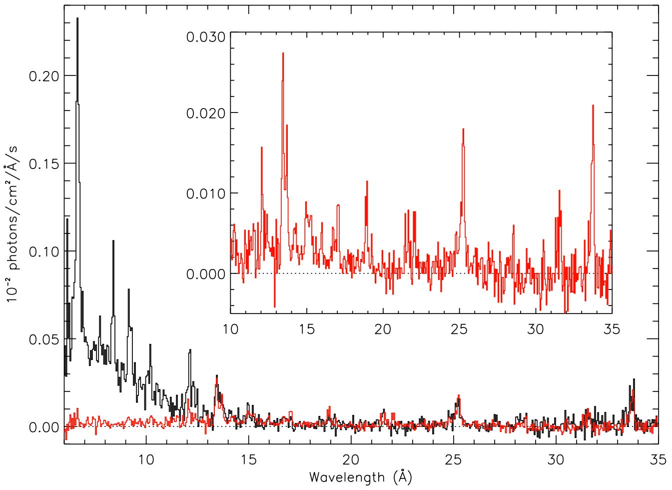

Figure 3. First order background subtracted RGS spectra, corrected for effective area. The black spectrum is from the observation at phase $\phi = 0.11$, and the gray spectrum from phase $\phi = 0.37$. The inset box is a blow up of the $\phi = 0.37$ observation.

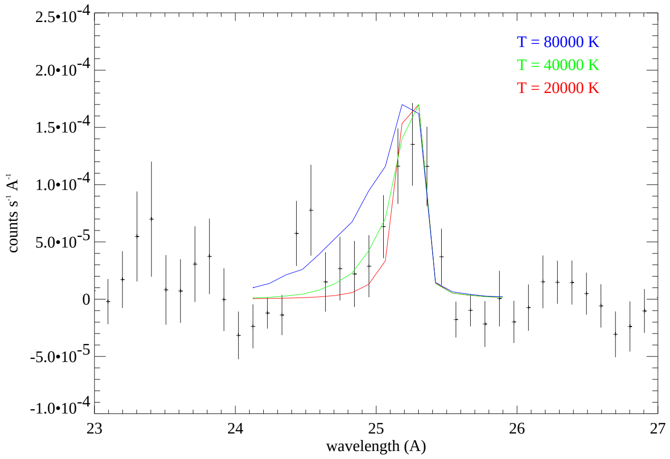

Figure 4. Observed RGS XMM-Newton spectrum around the C VI RRC compared with the theoretically calculated energy distribution for the three electron temperatures T_e = 20000 K, 40000 K, and 80000 K, folded with the RGS response function.

assuming an inclination of the orbital plane of $i = 65$. Analytical fits for the partial photoionization cross sections given by Verner & Yakovlev (1995) were used to attenuate the high state spectrum. The helium, carbon and oxygen abundances and their ionization state are taken from the spectroscopic analysis of the WR atmosphere by De Marco et al. (2000, model results 'ISA'). The neon abundance was set to the value determined from ISO-SWS spectroscopy Ne/He= $4 \cdot 10^{-3}$ by number (Dessart et al. 2000), assuming neon to be doubly ionized. The magnesium and silicon abundances were set to 1/10th of the neon abundance and for the sulfur abundance we chose 1/20th of the neon abundance.

As can be seen in Fig. 2 the absorption by the WR wind that is predicted by the WR model atmosphere is substantially too high. This is no surprise as the chosen WR model atmosphere assumes the WR wind to be homogeneous. However, nowadays it is agreed that stellar winds from massive stars are clumped. If we treat the column density as a free parameter and adjust it to fit the observed attenuation then we derive a column density of $5 \cdot 10^{21}$ cm^2, which is a factor 4 lower than what we predicted from the WR model.

4. The low energy emission lines

The calculations in the previous section showed that in the low state the WR wind absorbs all X-rays emerging from the wind collision zone for energies below 2 keV. Therefore, the low energy X-ray emission must originate from a different region than the collision zone. In Figs. 2 and 3 there is little flux variations longwards of 13 Å between observations at different orbital phases. Thus, these emission lines are formed either far out, such that any WR wind material between us and the emission region is optically transparent up to 35 Å or, the emission region is symmetric with regards to the orbital motion. The latter could be the case for radiative instabilities within the dominant WR wind. The former interpretation is the case if some outer regions of the WR wind are photoionized by the X-rays from the central collision zone. In particular, the part of the WR wind that winds around the cavity blown by the O star wind is at large distance from the origin of the stellar wind and therefore, the low wind density is not expected to absorb significantly emission arising from this region. However, through the cavity created by the O star wind, this region is exposed directly to the hard X-rays emerging from the collision zone.

The *XMM-Newton* spectra provide direct evidence that the carbon lines arise from a photoionized region. In the RGS spectra (Fig. 3) we see the Lyman series of C VI up to at least the C VI Lyγ line and in addition, we observe a strong radiative recombination continuum (RRC) at 25.3 Å. The intensities of the C VI emission lines and the RRC are in agreement with both being formed by recombination. The width of the RRC is a direct measure of the temperature of the recombining electrons. In Fig. 4 we compare the observed C VI RRC with the theoretically calculated spectral distribution for different electron temperatures. We conclude that electron temperatures below about 60 kK agree with the observed energy distribution.

5. Discussion

Our *XMM-Newton* observations provide direct evidence for X-ray emission emerging from the wind collision zone and from a cool region that is photoionized by X-rays, presumably by the radiation from the collision zone. We understand the observed variation in intensity between the spectra at low and high state to be due to a higher column density along the line of sight towards the wind collision zone. Because the WR wind is dominant over the O star wind the location of the wind collision zone must be very close to the O star. In Sect. 3 we derived that the observed column density towards the O star is a factor of 4 lower than what we predict from an unclumped model of the WR wind. As the predictions of atmosphere models depend on the square root of a clumping factor (defined as the ratio of the compressed density relative to the mean density) we conclude that the WR wind is clumped by a factor of 16.

In addition to the two emission regions for which we have direct observational evidence, i.e. the hard X-ray emitting collision zone and the photoionized cool region, we also expect to see X-rays from shocks intrinsic to the stellar wind from the WR star. In order to single out such lines we plot in Fig. 5 the emission measure of strong emission lines. It is evident that the group of the Ne X, Mg XI, and Fe XVII emission lines form at about the same temperature and volume. As the Ne X and Mg XI lines are only observable at high state and they are occulted at the other phases, these lines can be associated unambiguously with the wind collision zone. The two Fe XVII lines are also variable with phase at about a 50% level. It may well be that these relatively weak lines are blended and that only the variable part is due to the Fe XVII lines. Better candidates for lines that form by wind instabilities are the three lines in Fig. 5 that differ in temperature and emission measure from the wind collision lines.

The '*rif* components of the Ne IX triplet (G and R ratios) were analyzed by Skinner et al. (2001) who concluded that this line is formed at temperatures for which Ne IX has maximum emissivity, that the line ratio is consistent with its low density limit, and that there is negligible influence of an exiting radiation field. Consequently, the line must form at a large distance from the O star because otherwise, the stellar UV continuum would create deviations from the observed line ratios. Thus, the Ne IX line is a good candidate for being formed in shocks within the WR wind. However, we note that the deduced emission measure is surprisingly small if compared to the emission measure of the single O star ζ Pup (Kahn et al. 2001).

The emission measures of the oxygen lines in Fig. 5 are even smaller than that of the Ne IX line. The difference cannot be explained by an incorrectly adopted abundance ratio because in a WC wind both, O and Ne, can be expected to be overabundant by a factor of the order of 10, which would reduce the emission measures of all three lines by a similar factor. Therefore, it seems more plausible that the oxygen lines are not formed by shocks in the WR wind but are also associated to photoionization zone of the carbon lines. The question then arises why don't we observe oxygen lines emerging from wind instabilities or vice versa, what is the contribution to Ne IX from the photoionized region? The answewr to these questions must come from hydrodynamic simulations of the wind collision and subsequent radiation transport in a detailed geometry.

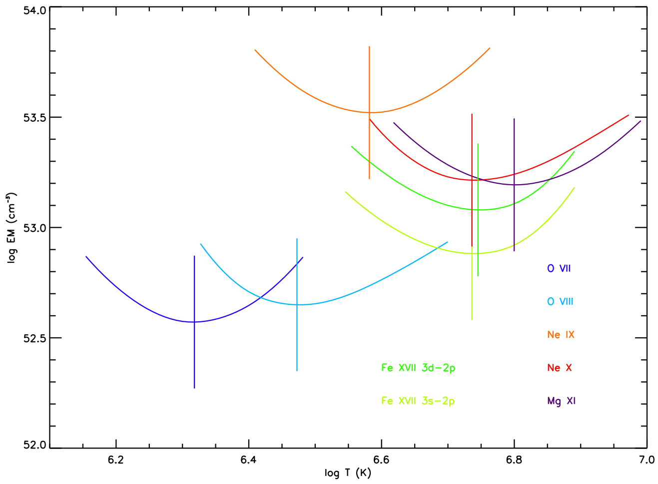

Figure 5. Emission measure distribution derived from the line fluxes of the high state observation. The abundances of neon and magnesium are adjusted to be $3\times$ solar, *while iron and oxygen are assumed to have solar abundance.*

Acknowledgements

This work is based on observations obtained with XMM-Newton, an ESA science mission with instruments and contributions directly funded by ESA Member States and the USA (NASA). M. A. acknowledges support from the Swiss National Science Foundation (grants 2100-049343 and 2000-058827)

References

De Marco O., Schmutz W. 1999, A&A 345, 163
De Marco O., Schmutz W., Crowther P.A., Hillier D.J., Dessart L., de Koter A., Schweickhardt J. 2000, A&A 358, 187
Dessart L., Crowther P.A., Hillier D.J. et al. 2000, MNRAS 315, 407
Folini D., Walder R. 2000. In: ASP Conf. Ser. 204, p. 267
den Herder J.W., Brinkman A.C., Kahn S.M., et al. 2001, A&A 365, L7
Jansen F., Lumb D. H., Altieri B., et al. 2001, A&A, 365, L1
Schaerer D., Schmutz W., Grenon M. 1997, ApJ 484, 153
Schmutz W., Schweickhardt J., Stahl O. et al. 1997, A&A 328, 219
Skinner S.L., Güdel M., Schmutz W., Stevens I.R. 2001, ApJL 558, L113
Stevens I.R., Corcoran M.F., Willis A.J., Skinner S.L., Pollock A.M.T., Nagase F., Koyama, K. 1996, MNRAS, 283, 589
Strüder L., Briel U. G., Dennerl K., et al. 2001, A&A 365, L18
Turner M.J.L., Abbey A., Arnaud M., et al. 2001, A&A, 365, L27
van der Hucht K. A., Schrijver H., Stenholm B., et al. 1997, New Astron. 2, 245
Verner, D. A. & Yakovlev D. G. 1995, A&AS 109, 125
Walder R., Folini D., Motamen S.M. 1999. In: IAU Symp. 193, p. 298
Willis A.J., Schild H., Stevens I.R. 1995, A&A 298, 549